

FAST TRACK COMMUNICATION

Coherent control of electron wave packets in dissociating H_2^+

Feng He¹, Camilo Ruiz² and Andreas Becker

Max-Planck-Institut für Physik komplexer Systeme, Nöthnitzer Str.38, D-01187 Dresden, Germany

Received 8 January 2008

Published 3 April 2008

Online at stacks.iop.org/JPhysB/41/081003**Abstract**

Coherent control of electron localization in the dissociation of a hydrogen molecular ion exposed to an attosecond pulse train and a time-delayed near-infrared laser pulse are studied by solving numerically the time-dependent Schrödinger equation. The attosecond pulses in the train generate a train of electron wave packets in the dissociating molecular ion, which are steered by the near-infrared laser field between the two nuclei. Our results show that a large asymmetry in the total electron localization can be achieved if the attosecond pulses are separated by a full cycle of the near-infrared pulse, while the asymmetry and the degree of control are much smaller for a pulse separation of half a cycle. The analysis of results reveals an efficient control mechanism on a timescale of few femtoseconds via the time-delay and the carrier-to-envelope phase of the near-infrared pulse.

(Some figures in this article are in colour only in the electronic version)

Controlling a chemical reaction with lasers has been a goal in physics and chemistry for decades. Bond breaking and forming in a molecule is an ultrafast dynamic process involving motion of electrons and atomic nuclei in the target. Using a time resolution of femtosecond laser pulses it has become possible to control the dynamics on the timescale of nuclear motion. This enables us nowadays to target one atom in a molecule and selectively break its bonds with a certain probability [1]. Prominent control schemes are based on the time delay between two pulses [2, 3], multiple-path interference [4] or stimulated Raman adiabatic passage [5]. With the technological progress to change the spectral phases and amplitudes of the different frequency components of a laser pulse, the range of femtosecond control schemes has been further extended [6, 7].

Recent few-cycle and sub-femtosecond UV pulses [8–11] provide a time resolution beyond the limit of nuclear motion and enable the observation of electron dynamics in an atom or molecule, such as strong-field ionization dynamics [12, 13] and electron correlation [14]. Concepts of controlling electron

dynamics in a reaction using these new laser technologies were proposed for the first time recently. They deal with the simplest process, namely the localization of an electron in the dissociating hydrogen molecular ion, which has been studied both in theory [15–18] and experiment [19]. The control of the electron dynamics via the field has been achieved either by the phase between the envelope and the carrier frequency of a single few-cycle pulse [15, 16, 18, 19] or by the time delay of two coherent ultrashort laser pulses [17]. In the latter approach a first (sub-)femtosecond ultraviolet pulse excites the electron wave packet to a dissociating state in H_2^+ , while a second time-delayed near-infrared pulse steers the electron between the two dissociating nuclei. This strategy appears to be very efficient, as probabilities of localizing the electron at one of the two nuclei of 85% and more have been found in *ab initio* numerical simulations.

In this communication we extend the two-pulse strategy by using attosecond pulse trains instead of an isolated single attosecond pulse for the excitation step. Isolation of a single attosecond pulse can be realized today with state of the art experiments by either selecting high-energy cutoff harmonics from a few-cycle pulse [9, 20] or by using polarization gating technique [21–25]. More easily obtained are the attosecond pulse trains, as they are produced in infrared laser pulses of

¹ Present address: James R Macdonald Laboratory, Kansas State University, Manhattan, Kansas 66506-2604, USA.

² Present address: Blackett Laboratory, Imperial College London, London SW7 2BW, UK.

many-cycles. In this case the pulses are separated by half a period of the driving pulse [26]. Besides that, trains of attosecond pulses with only one pulse per infrared laser cycle can be produced if the atomic gas is exposed to an infrared laser field and its second harmonic [27, 28]. Next we will study, on the basis of results of numerical simulations, how such pulse trains can be used to generate trains of electron wave packets on the dissociating $2p\sigma_u$ state of H_2^+ . These wave packets are then directed by a time-delayed infrared laser pulse either to opposite nuclei or to the same nucleus in the dissociating molecular ion.

In numerical simulations we have used a three-dimensional model of hydrogen molecular ion interacting with a sequence of linearly polarized intense laser pulses at different frequencies. The H_2^+ ion is considered to be aligned along the polarization axis of the lasers, rotation of the internuclear axis is not taken into account. The nuclear motion is therefore restricted along the internuclear axis, while the electronic motion is symmetric about the polarization direction. The corresponding three-dimensional time-dependent Schrödinger equation can be written as (Hartree atomic units, $e = m = \hbar = 1$ are used):

$$i\frac{\partial}{\partial t}\Phi(R, z, \rho; t) = [H_0 + V(t)]\Phi(R, z, \rho; t), \quad (1)$$

with

$$H_0 = -\frac{1}{M}\frac{\partial^2}{\partial R^2} - \frac{1}{2\mu}\left(\frac{\partial^2}{\partial z^2} + \frac{\partial^2}{\partial \rho^2} + \frac{1}{\rho}\frac{\partial}{\partial \rho}\right) + \frac{1}{\sqrt{R^2 + \beta}} - \frac{1}{\sqrt{(z + \frac{R}{2})^2 + \rho^2 + \alpha}} - \frac{1}{\sqrt{(z - \frac{R}{2})^2 + \rho^2 + \alpha}}, \quad (2)$$

where R is the internuclear distance, M is the mass of the proton and $\mu = 2M/(2M + 1)$ is the reduced electron mass. Two soft-core parameters $\alpha = 0.0109$ and $\beta = 0.1$ are chosen to soften the singularities of the Coulomb potentials and to yield the experimental ground state energy and equilibrium distance of -0.6028 a.u. and 2.0 a.u., respectively. The time-dependent potential due to the interaction with the external laser pulses is given in length gauge as

$$V(t) = E(t)\left(1 + \frac{1}{1 + 2M}\right)z \quad (3)$$

with

$$E(t) = E_{as1} \exp\left[-8 \ln 2 \left(\frac{t + \frac{\delta t}{2}}{\tau_{as}}\right)^2\right] \sin\left[\omega_{as}\left(t + \frac{\delta t}{2}\right) + \phi_{as}\right] + E_{as2} \exp\left[-8 \ln 2 \left(\frac{t - \frac{\delta t}{2}}{\tau_{as}}\right)^2\right] \sin\left[\omega_{as}\left(t - \frac{\delta t}{2}\right) + \phi_{as}\right] + E_{ir} \exp\left[-8 \ln 2 \left(\frac{t - \Delta t}{\tau_{ir}}\right)^2\right] \sin[\omega_{ir}(t - \Delta t) + \phi_{ir}], \quad (4)$$

where $E_{as1,as2,ir}$, $\tau_{as,ir}$, $\omega_{as,ir}$ and $\phi_{as,ir}$ are the amplitude, pulse width, frequency and carrier-to-envelope phase of the attosecond and near-infrared pulses, respectively. δt and Δt are time delays between the attosecond pulses and between

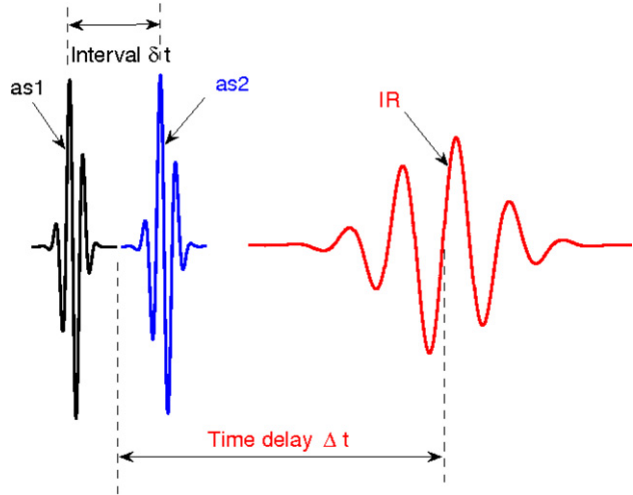


Figure 1. Control scheme with an attosecond pulse train of two pulses (as 1 and as 2) separated in time by δt and a near-infrared pulse (ir) with a time delay of Δt to the center of the attosecond pulse train. The attosecond pulses are used to generate electron wave packets on the $2p\sigma_u$ state of H_2^+ while the near-infrared pulse drives wave packets between the two nuclei.

the near-infrared and the center of the two attosecond pulses respectively.

As shown in figure 1, we have considered the shortest pulse train consisting of just two attosecond pulses separated by δt . In the present control strategy these pulses are used to generate electron wave packets on the dissociative $2p\sigma_u$ state. To this end, we have chosen the wavelength of the pulses as $\lambda_{as} = 115$ nm, which corresponds to the 7th harmonic of a near-infrared laser pulse operating at $\lambda_{ir} = 800$ nm. The photon energy of the attosecond pulses is approximately equal to the energy gap between the ground and the first excited states in our model. In simulations the other parameters of the pulses in the train were $I_{as1} = I_{as2} = 10^{13}$ W cm $^{-2}$ and $\tau_{as} = 0.76$ fs (two cycles, FWHM). Two intervals $\delta t = T_{ir}$ and $\delta t = T_{ir}/2$ have been considered, where T_{ir} is the period of the near-infrared laser field, corresponding either to one or two attosecond pulses per cycle of the driving pulse. In test calculations we have found that results do not depend on the carrier-to-envelope phase of the attosecond pulses, we have chosen $\phi_{as} = 0$ in the present simulations. As outlined above, the near-infrared laser pulse, delayed by Δt to the center of the attosecond pulse train, is used to steer electron wave packets between the dissociating nuclei. We have chosen an intensity of $I_{ir} = 3 \times 10^{12}$ W cm $^{-2}$ and a width of $\tau_{ir} = 8$ fs (three cycles, FWHM). The intensity is on one hand high enough to provide an effective control of the electron wave packets and on the other weak enough to avoid significant additional dissociation or ionization of the H_2^+ ion.

The time-dependent Schrödinger equation has been solved using Crank–Nicholson method. The initial state of the hydrogen molecular ion (electronic and vibrational ground state, $1s\sigma_g, v = 0$) has been obtained by an imaginary time propagation. The sizes of the simulation box were 0 to 20 a.u., -30 to 30 a.u., and 0 to 24 a.u. in R, z and ρ directions, which were sampled by 500, 200 and 80 points, respectively.

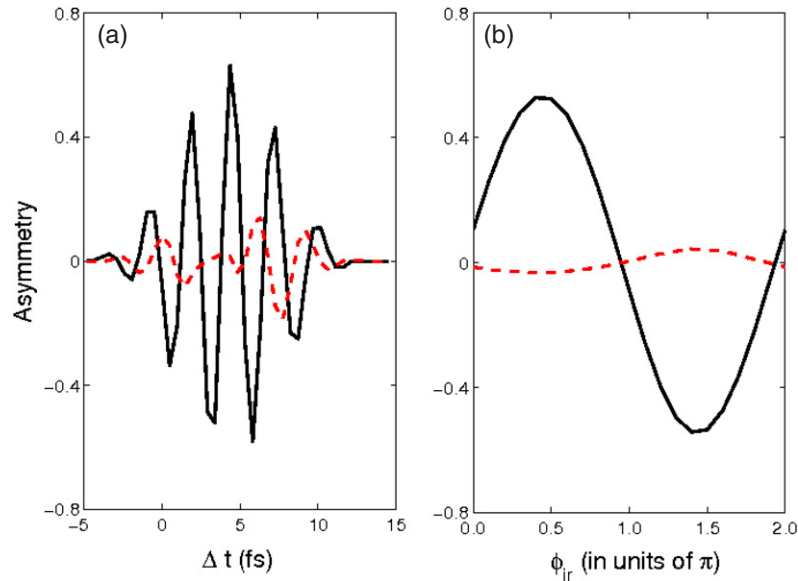


Figure 2. Asymmetry parameter A as a function of, (a) the time delay Δt , and (b) the carrier-to-envelope phase of the near-infrared laser pulses for $\delta t = T_{ir}$ (solid lines) and $\delta t = T_{ir}/2$ (dashed lines).

The time step in the simulations was 0.1 a.u.. The outgoing parts of the wavefunction have been absorbed at edges of the grid via a $\cos^{1/6}$ mask function. The probabilities of electron localization at either one of the protons, P_+ and P_- , have been defined via the probability densities in areas of the numerical grid as

$$P_+ : R > 10 \quad \text{and} \quad \sqrt{(z - R/2)^2 + \rho^2} < 5, \quad (5)$$

$$P_- : R > 10 \quad \text{and} \quad \sqrt{(z + R/2)^2 + \rho^2} < 5. \quad (6)$$

Absorbed contributions have been stored and added to the respective electron localization probabilities. The asymmetry in the electron localization is given by

$$A = \frac{P_- - P_+}{P_- + P_+}. \quad (7)$$

In our previous studies using an isolated attosecond pulse for the excitation of the electron wave packet [17] we have found that the localization of the electron can be controlled by the time delay and the carrier-to-envelope phase of the steering near-infrared pulse. We therefore present in figure 2 the asymmetry parameter A , obtained for the present extended control scheme, as a function of (a) the time delay Δt ($\phi_{ir} = 0$) and (b) the carrier-to-envelope phase ϕ_{ir} ($\Delta t = 2.4$ fs) of the near-infrared pulse. For a separation of $\delta t = T_{ir}$ between the attosecond pulses (solid lines) the asymmetry parameter A shows strong variations with a maximum of $A_{\max} = 0.6$, corresponding to an electron localization probability of 80%. In contrast, for $\delta t = T_{ir}/2$ the asymmetry (dashed lines) is much smaller (close to zero) for all time delays and phases considered, indicating a small degree of control of the total electron localization.

In order to understand the difference between the two scenarios we have repeated the calculations but deliberately switched off one of the two attosecond pulses in the train, which is done by setting $E_{as1} = 0$ or $E_{as2} = 0$. Thus, in

each of these additional simulations excitation occurs via a single isolated attosecond pulse only. In agreement with our previous findings [17], the results of all these calculations (cf left-hand column of figure 3) show a strong variation of the individual asymmetry parameters $A_{E_{as1}=0}$ (solid lines) and $A_{E_{as2}=0}$ (dashed lines). In figure 3 it is shown the dependence of the asymmetry on the time delay Δt at $\phi_{ir} = 0$. Similar strong variations of $A_{E_{as1}=0}$ and $A_{E_{as2}=0}$ as a function of ϕ_{ir} at a fixed time delay Δt have been found (not shown). As can be seen from the comparison of the two scenarios, $\delta t = T_{ir}$ (figure 3(a)) and $\delta t = T_{ir}/2$ (figure 3(c)), in the former (latter) case the individual electron wave packets are directed to the same nucleus (opposite nuclei). Consequently, the averaged asymmetry parameter $A_{\text{avgd}} = (A_{E_{as1}=0} + A_{E_{as2}=0})/2$ shows either the same strong variation (figure 3(b), solid line) or almost vanishes (figure 3(d), solid line). Please note that the averaged values are found to agree well with the asymmetry parameters obtained in the full simulations, which, for the sake of comparison, are replotted in figures 3(b) and (d) (dashed line with circles). The test calculations can be therefore used to understand results of the full simulations as follows: in both scenarios two separate electron wave packets are generated by the two attosecond pulses. While for $\delta t = T_{ir}/2$ the two wave packets are directed by the near-infrared pulse to opposite directions (nuclei), for $\delta t = T_{ir}$ both wave packets are steered in the same direction and therefore to the same nucleus. As a result in the former case the asymmetry parameter almost vanishes but not in the latter scenario.

The good agreement between the asymmetry parameters, obtained in the full simulations and the averaged value in the test simulations, in figures 3(b) and (d) further indicate that interference effects between the electron wave packets generated on the dissociative $2p\sigma_u$ state by the two attosecond pulses do not play a major role. This is due to the strong confinement of the wave packets, which is produced by the

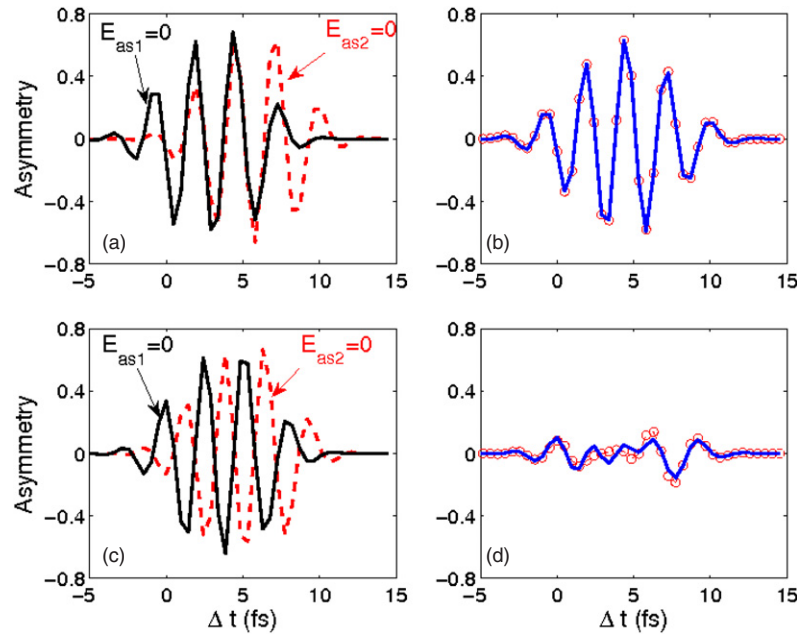


Figure 3. Asymmetry parameter as a function of the time delay Δt for the two scenarios ($\delta t = T_{ir}$ (panels in upper row) and $\delta t = T_{ir}/2$ (panels in the lower row)). Left-hand column: results of calculations in which one of the two attosecond pulses are switched off, namely $E_{as1} = 0$ (solid line) and $E_{as2} = 0$ (dashed line). Right-hand column: comparison of the asymmetry parameter $A_{\text{avrgd}} = (A_{E_{as1}=0} + A_{E_{as2}=0})/2$ (solid line) with the results of the full calculations, in which both attosecond pulses are switched on (dashed line with circles).

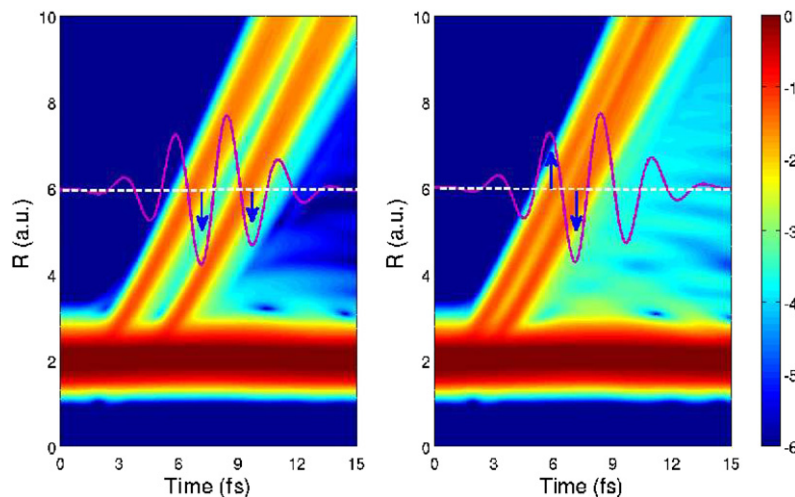


Figure 4. Distribution $P(R, t)$ for $\delta t = T_{ir}$ (left-hand panel) and $\delta t = T_{ir}/2$ (right-hand panel) with $E_{ir} = 0$.

short time duration of the attosecond pulses [29]. It can be seen from probability distributions,

$$P(R, t) = \iint |\phi(R, z, \rho; t)|^2 dz d\rho, \quad (8)$$

shown in figure 4 for $\delta t = T_{ir}$ (left hand panel) and $T_{ir}/2$ (right hand panel). The results have been obtained for $E_{ir} = 0$ in order to analyze the dynamics of the two electron wave packets. In both cases, the distribution is initially located around $R = 2$ a.u., which is the equilibrium distance of the initial ground state, and the two dissociating wave packets are seen propagating to larger internuclear distances. Indeed, the wave packets are rather well separated even for the shorter

time delay of $\delta t = T_{ir}/2$ between the two attosecond pulses. This allows for the coherent control of the wave packets by the near-infrared field separately, as indicated by the solid lines and the arrows.

We expect that the results presented above can be generalized for pulse trains with more than two attosecond pulses. If the interval between the attosecond pulses is nT_{ir} (n is a natural number), each generated electron wave packet is directed to the same nucleus, providing an efficient control of the electron localization. On the other hand, if the attosecond pulses in the train are separated by $(n-1/2)T_{ir}$, the subsequent electron wave packets will be directed to opposite directions

and, hence, the electron localization probabilities at the two nuclei will be almost equal. Consequently, the asymmetry and the total degree of control will be rather small. We may finally note that we have considered attosecond pulses with constant peak intensity in the train. Experimentally, the intensities usually differ from pulse to pulse. This will lead to different probabilities of the individual electron wave packets and, hence, influence the total asymmetry. However, we may expect that our general conclusions for pulse trains with one or two pulses per near-infrared laser cycle will still hold.

In conclusion, we have studied the control of electron wave packets during the dissociation of the hydrogen molecular ion exposed to an attosecond pulse train and a near-infrared laser pulse. It is found that a high degree of control can be achieved if the pulses in the train are separated by one cycle of the near-infrared laser, but a considerably lower one if the separation is just half a cycle. Our analysis has shown that this is due to the fact that in the former scenario each electron wave packet is directed to the same direction (nucleus) while in the latter subsequent wave packets are steered in opposite directions (nuclei). This extension of the control scheme lowers the technical requirements for the experiment, as an attosecond pulse train is commonly obtained in a strong field experiment.

Acknowledgments

The simulations have been performed using the virtual laser lab ‘Nonlinear Processes in Strong Fields Library’, we thank S Baier, P Panek, and A Requate for their contributions to this numerical library. Partial support from DAAD (Project No. D/05/25690) is acknowledged.

References

- [1] Zewail A H 2000 *J. Phys. Chem. A* **104** 5660
 [2] Tannor D J and Rice S A 1985 *J. Chem. Phys.* **83** 5013

- [3] Tannor D J, Kosloff R and Rice S A 1986 *J. Chem. Phys.* **85** 5805
 [4] Shapiro M and Brumer P 1986 *J. Chem. Phys.* **84** 4103
 [5] Bergmann K, Theuer H and Shore B W 1998 *Rev. Mod. Phys.* **70** 1003
 [6] Judson R S and Rabitz H 1992 *Phys. Rev. Lett.* **68** 1500
 [7] Assion A, Baumert T, Bergt M, Brixner T, Kiefer B, Seyfried V, Strehle M and Gerber G 1998 *Science* **282** 919
 [8] Baltuska A *et al* 2003 *Nature* **42** 611
 [9] Kienberger R *et al* 2004 *Nature* **427** 817
 [10] Goulielmakis E *et al* 2004 *Science* **305** 1267
 [11] Hauri C P, Kronelis W, Helbing F W, Heinrich A, Couairon A, Mysyrowicz A, Biegert J and Keller U 2004 *Appl. Phys. B* **79** 673
 [12] Johnsson P *et al* 2005 *Phys. Rev. Lett.* **95** 013001
 [13] Uiberacker M *et al* 2007 *Nature* **446** 627
 [14] Hu S X and Collins L A 2006 *Phys. Rev. Lett.* **96** 073004
 [15] Roudnev V, Esry B D and Ben-Itzhak I 2004 *Phys. Rev. Lett.* **93** 163601
 [16] Tong X M and Lin C D 2007 *Phys. Rev. Lett.* **98** 123002
 [17] He F, Ruiz C and Becker A 2007 *Phys. Rev. Lett.* **99** 083002
 [18] Graefe S and Ivanov M Yu 2007 *Phys. Rev. Lett.* **99** 163603
 [19] Kling M F *et al* 2006 *Science* **312** 246
 [20] Hentschel M, Kienberger R, Spielmann Ch, Reider G A, Milosevic N, Brabec T, Corkum P, Heinzmann U, Drescher M and Krausz F 2001 *Nature* **414** 509
 [21] Corkum P B, Burnett N H and Ivanov M Yu 1994 *Opt. Lett.* **19** 1870
 [22] Strelkov V, Zair A, Tcherbakoff O, López-Martens R, Cormier E, Mével E and Constant E 2004 *Appl. Phys. B* **78** 879
 [23] Sola I J *et al* 2006 *Nature Phys.* **2** 319
 [24] Sansone G *et al* 2006 *Science* **314** 443
 [25] He F, Ruiz C and Becker A 2007 *Opt. Lett.* **32** 3224
 [26] Paul P M, Toma E S, Breger P, Mullot G, Aude F, Balcou Ph, Muller H G and Agostini P 2001 *Science* **292** 1689
 [27] Mauritsson J, Johnsson P, Gustafsson E, L’Huillier A, Schafer K J and Gaarde M B 2006 *Phys. Rev. Lett.* **97** 013001
 [28] Dudovich N, Smirnova O, Levesque J, Mairesse Y, Ivanov M Yu, Villeneuve D M and Corkum P B 2006 *Nature Phys.* **2** 781
 [29] He F and Becker A 2008 *J. Phys. B: At. Mol. Opt. Phys.* **41** 074017